Istrazivanja i projektovanja za privredu
Journal of Applied Engineering Science

Original Scientific Paper

doi:10.5937/jaes18-24459

Paper number: 18(2020)3, 712, 443 - 457

STRUCTURAL ANALYSIS OF BUILT-UP MEMBERS WITH ANGLES

Claudio Bernuzzi[1]*, Elisa Bertinotti[2], Marco Simoncelli[1]

[1]Politecnico di Milano, Faculty of civil engineering, Department of Architecture, Built environment and Construction engineering (ABC), Milano, Italy

[2]Structural engineer, Freelancer, Novara, Italy

Built-up steel members are frequently used in lifting equipment structures, such as tower cranes, gantry cranes, mobile cranes jibs and so on. Mining stiffleg derricks are the subject of the present paper. Derricks design is usually carried out using commercial finite element analysis packages (FEAP): these packages often offer only beam formulations developed for bi-symmetric cross-section members. So, important effects associated with buckling interaction between axial force and bending moments, as well as with the presence of warping torsion, are currently neglected in analysis design. Moreover, these interactions are not yet included in standard provisions.

The paper is focused on built-up members for stiffleg derricks made by angles, focusing on the analysis phase. Key features of single angles are presented, stressing out the importance of capturing the buckling loads for compression, bending and compression plus bending. An applicative part is also proposed: two stiffleg derricks, differing only in panel geometry, have been studied, considering each in six geometrical configurations. Structural analyses have been carried out by using two FEAPs differing for the degree of refinement of the implemented beam formulations. Research outcomes highlight the important influence of effects that are currently neglected in routine design.

Key words: stiffleg derrick, angle, buckling analysis, axial force–bending moment interaction, warping torsion, bimoment

INTRODUCTION

Built-up steel members are frequently used in civil and industrial engineering structures: also, many types of lifting devices are formed by built-up members [1], such as tower and gantry cranes, portal cranes, mobile cranes jibs and derricks cranes. Attention is herein focused on stiffleg derrick cranes with angles, simply identified hereinafter as derricks. Due to their high lifting capacity, derricks are widely used for handling heavy loads, both in maritime and mining sectors, as well for construction of special plants and wherever required load capacity cannot be guaranteed by other solutions

Figure 1 shows main structures of a derricks crane: the boom is supported by a vertical tower, whose top is linked with two rigid inclined legs (tie-rods or stiff legs). The angles between tie-rods is 90° in the horizontal plane and 45° between tie-rods and tower in the vertical plane. All the structural components are generally steel built-up modular members, usually designed to comply with the limit profile for standard road transportation. The modules, built in factory, are assembled on site by means of preloaded bolted splice connections. As they are stationary equipments, derricks are mounted on a reinforced concrete foundation or directly fixed to the rock.

Derricks are equipped with three groups of mechanisms, one for each possible movement: rotation, luffing and lifting. A slewing wheel placed at the bottom of the tower enables the rotation of the tower together with the boom in the horizontal plane; thanks to a system of multiple ropes running from the base of the tower to its top, boom can luffing in vertical plane. Finally, another system of multiple ropes running from the base of the tower to the top of the boom enables the lifting of the loads.

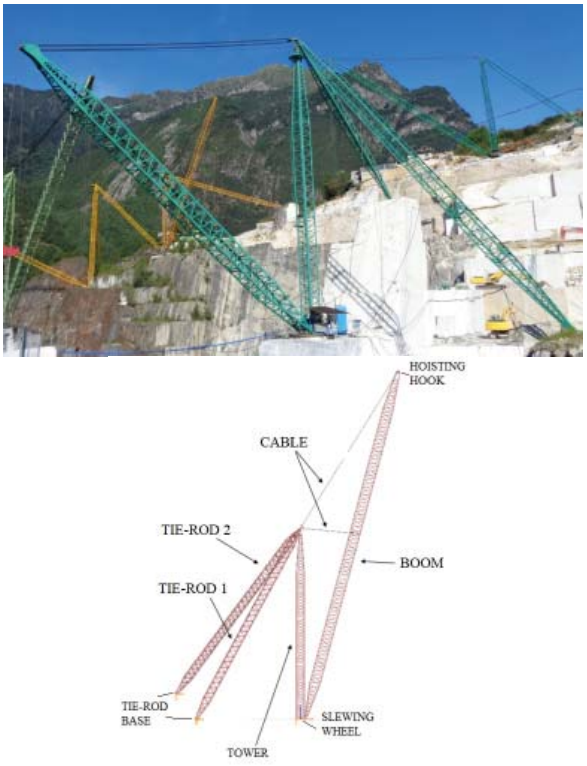

Figure 1: Typical stiffleg derrick (a) its main components (b)

**claudio.bernuzzi@polimi.it*

Figure 2: Typical detail of the connection between diagonals and strut

Rotation and luffing movements generate different geometrical configurations, each of them creating different stresses in the structures.

The maximum derrick load capacity directly depends on the boom inclination: usually, from an inclination of 15° to 80° respect to the vertical axis, the load capacity reduces about 1.5 times.

In design analysis, stresses are usually evaluated by using commercial finite element analysis packages (FEAPs): FE beam elements are used in modelling each derrick component, owing to the presence of wall rods welded to the chords (fig. 2). Resulting mesh, consisting of several hundreds of elements, is usually adequately refined.

Design strategies [2,3] currently adopted are based on rules codified for traditional steel carpentry frames, usually realized with bi-symmetric cross-section elements: so, using such rules, buckling interaction between axial force and bending moments is totally neglected. Assessing a nil warping constant leads to the absence of bimoment in the set of the generalized output forces, so that key features of angles behaviour are not adequately taken into account.

This paper deals with derricks structural analysis. Two stiffleg derricks have been modelled via two commercial FEAPs, differing each other for presence or absence of the cross-section warping as additional degree of freedom in the FE beam formulation. Neither calculation criteria nor assessment about fatigue are here discussed: attention has been focussed on buckling conditions and key features of single angles. Importance of both flexural-torsional buckling mode and of interaction between axial force and bending moments have been stressed out. Finally, the design generalized forces associated with the two FE beam formulation have been compared, considering six different geometrical configurations. Warping effects have been directly appreciated, contrary to what generally happens in routine design and verification checks.

THE CONSIDERED DERRICKS

Two derricks (herein identified as A- and B-type) have been the object of numerical application in this study. For both derrick A-type and B-type maximum load capacity is 50 tons, boom length is 60 m, tower height is 40 m and tie rods the length is 47 m. A structural steel of S275 grade has been used for all components.

A-type and B-type derricks differ only in panel geometry, more precisely in the number of legs per cross-section interested by diagonal connections. Figure 3 shows panel geometries: in the A-type one leg for cross-section is connected to the diagonals, in the B-type the diagonals of two perpendicular planes are connected at the same cross-section of the chord. In both types, all the member connections have been considered rigid joint, owing to the presence of welded details figure 2.

The A-type is an existing derrick, installed in a marble quarry on Italian Alps, while B-type is here just a model, considered in order to have a comparative case study regarding the influence of panel geometry.

In routine design, due to the presence of welded connections, derrick components have been entirely modeled with FE beam elements. Figure 4 shows the model, together with details on the angle cross-sections; according to the EC3 classification criteria [4], all angles are in class 1. About connections, on the top of the tower at joining with the tie rods, a perfect bi-directional hinge has been modelled, in order to leave free all the rotations. At the base of boom and tie-rods the rotations are admitted only in one direction and all the translations are fixed. The base of the tower is completely fixed with an eccentricity “e” from the base of the boom.

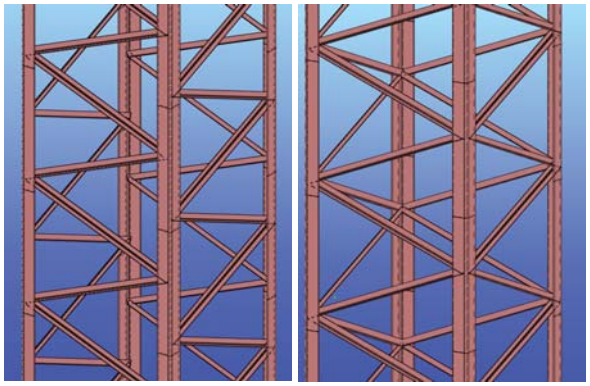

Figure 3: The considered derrick panels

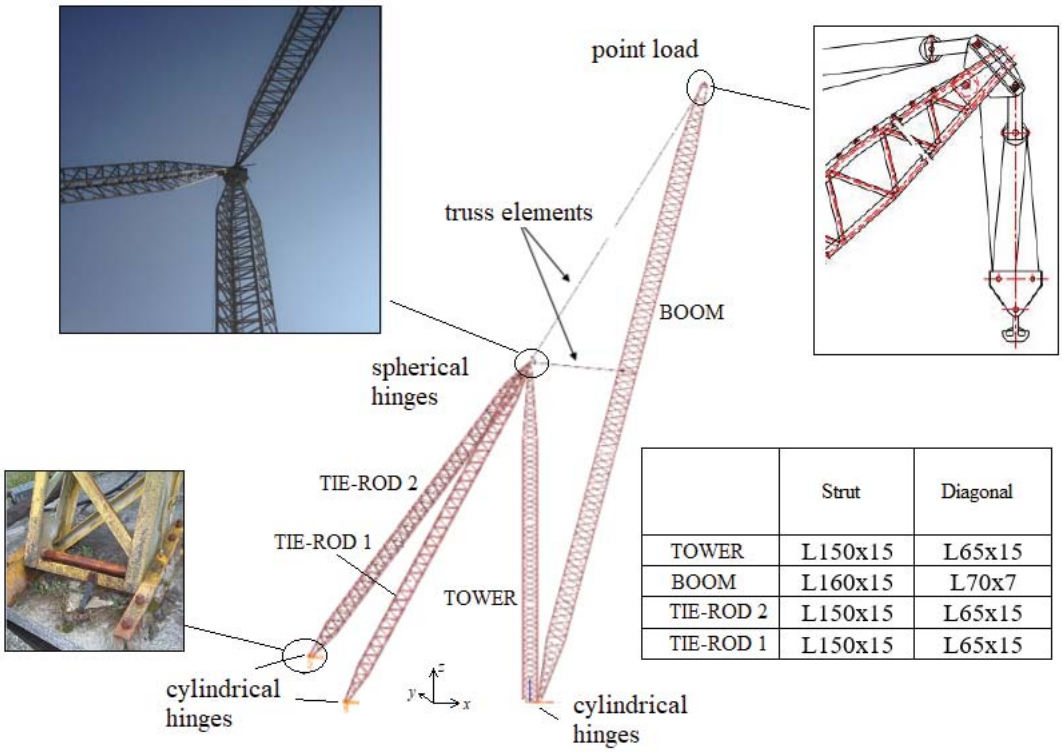

	Strut	Diagonal
TOWER	L150x15	L65x15
BOOM	L160x15	L70x7
TIE-ROD 2	L150x15	L65x15
TIE-ROD 1	L150x15	L65x15

Figure 4: Modelling details and cross-section dimensions

Due to derrick geometry, three symmetric (SB) and three non-symmetric (NS) configurations have been considered: in SB configurations the boom is located at the bisector of the angle between tie-rods, while in NS configurations the boom is located near a tie-rod. For both configuration, three different values of boom inclination with respect to the vertical axis have been considered (figure 5).

Numerical applications are herein discussed for the following modelled geometries:

- symmetric configuration on the horizontal plane (SB):
  - SB15: boom inclined of 15°;
  - SB65: boom inclined of 65°;
  - SB80: boom inclined of 80;
- non-symmetric configuration on the horizontal plane (NS):
  - NS15: boom inclined of 15°;
  - NS65: boom inclined of 65°;
  - NS80: boom inclined of 80°.

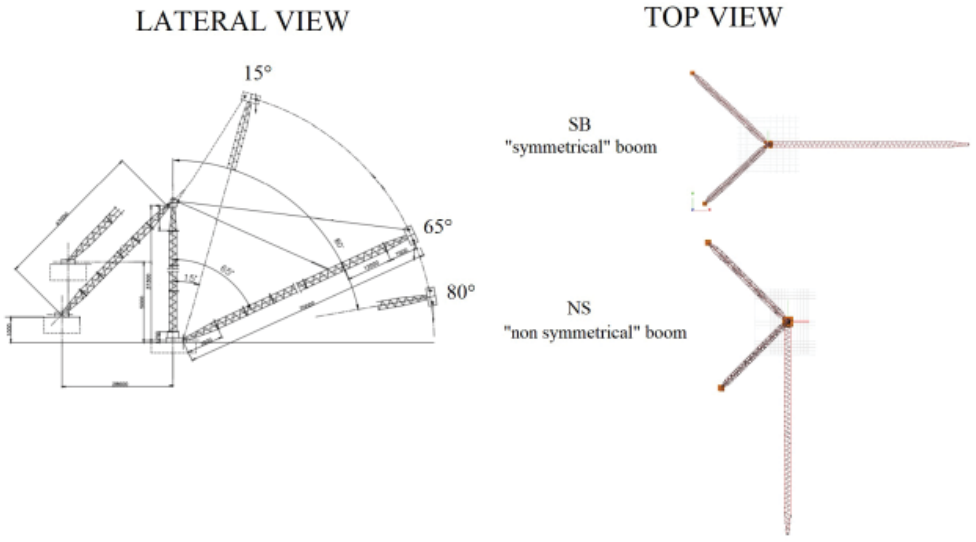

Figure 5: The considered derrick configurations

Second order and buckling analyses have been carried out by means of two commercial FEAPs: SAP2000 [5] and ConSteel [6]. The former offers the traditional 6DOFs beam element, the latter enables for structural analysis including effects associated with the 7th DOF (i.e. the cross-section warping). The same mesh has been used in both FEAPs. Model is characterized by 2200 nodes and 360 FE beams for the boom, 121 for the tower and 630 for the two tie-rods; each cable has been modelled via 3 truss elements.

REMARKS ON MONO-SYMMETRIC CROSS-SECTION MEMBERS

FEAPs commonly adopted in routine design generally offer beam elements characterized by 6 degrees of freedom (DOFs) per node [7]: such formulation is often adequate for structures realized by bi-symmetric cross-section elements. Anyway, in case of elements with a single axis of symmetry, a more refined FE beam formulation is required. As alternative to modelling the whole structure by using shell and/or solid elements, the so-called 7DOF FE beam formulation [8,9] can succesfully be used in order to consider the warping of the cross-section (θ). This additional DOF (i.e. the 7th one) is defined, on the basis of the torsional rotation (φ_x) as:

$$\theta = \theta(x) = \frac{-d\varphi_x}{dx} \tag{1}$$

Warping effects can be caught by means of 7DOF FE formulation, this resulting very efficient for the most common types of mono-symmetric cross-section members. 7DOF FE also accounts for the coupling between axial force and bending moments in buckling conditions: hence, it can also efficiently be used for bi-symmetric beam-columns, where non-negligible interaction is not jet included in design provisions and in routine design.

In every mono-symmetric cross-sections [10,11], owing to the eccentricity between the shear centre (*S*) and the centroid (*O*), reference has to be made to the shear centre for the definition of the whole set of generalized displacements, except than for the axial displacement u, related to the centroid (figure 6b). Moreover, as in traditional 6DOFs formulation, bending moments (M_y and M_z) and axial force (*N*) are referred to point *O*, while bimoment (*B*), shear forces (F_y and F_z) and uniform torsion moment (M_x) are related to point *S*. If *j* and *k* identify the end nodes of the FE *beam*, the algebraic linear system can be written in a general form as:

$$\begin{bmatrix} [K]^E_{jj} & [K]^E_{jk} \\ [K]^E_{kj} & [K]^E_{kk} \end{bmatrix} \begin{bmatrix} \{u\}_j \\ \{u\}_k \end{bmatrix} = \begin{bmatrix} \{f\}_j \\ \{f\}_k \end{bmatrix} \tag{2}$$

With respect to the more general case of a 7DOF beam formulation, the nodal displacement vector, $\{u\}_{j,k}$ and the associated force vector, $\{f\}_{j,k}$ can be expressed (figure 6) as:

$$\{u\}_{j,k} = \begin{bmatrix} u \\ v \\ w \\ \varphi_x \\ \varphi_y \\ \varphi_z \\ \theta \end{bmatrix} \tag{3a}$$

$$\{f\}_{j,k} = \begin{bmatrix} N \\ F_y \\ F_z \\ M_x \\ M_y \\ M_z \\ B \end{bmatrix} \tag{3b}$$

The presence of both terms θ and B characterizes only FE beam formulations, including the additional warping DOF (i.e. the 7DOFs one). With reference to a beam element of length *L*, considering its area (*A*), second moments of area (I_X and I_y) along principal axes, uniform torsion constant (I_t) and warping torsion constant (I_w) and assuming *E* and *G* as Young modulus and the shear

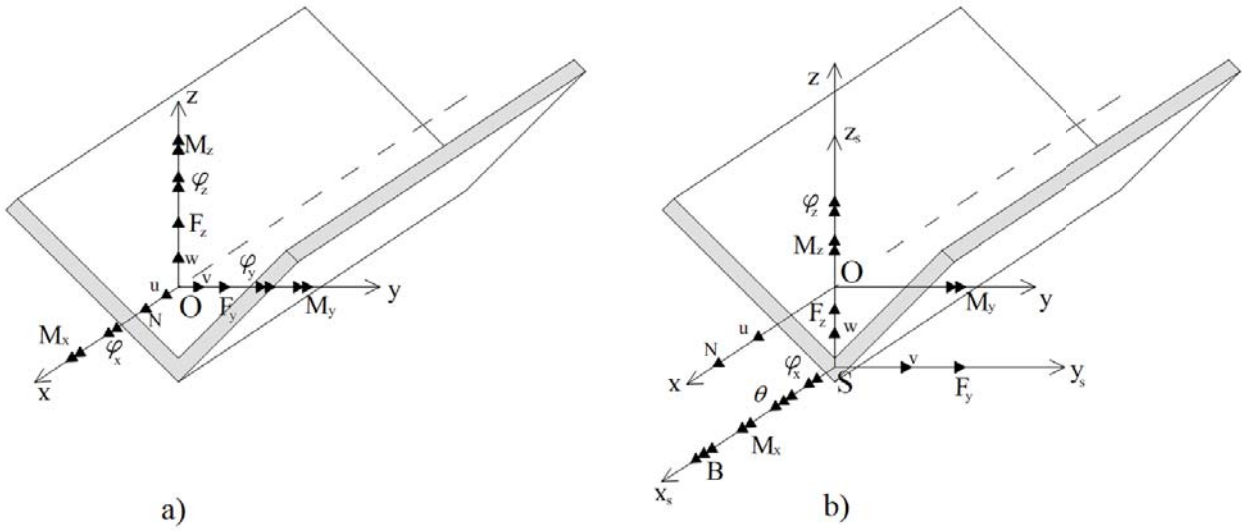

Figure 6: a) six and b) seven DOFs formulations

material modulus, respectively, the elastic stiffness sub-matrices $[K]_{jj}^{E}$ and $[K]_{j\bar{k}}^{E}$ can be defined as:

$$[K]_{jj}^{E}=\left[\begin{array}{cccccc|c} \frac{EA}{L} & 0 & 0 & 0 & 0 & 0 & 0 \\ & \frac{12EI_y}{L^3} & 0 & 0 & 0 & \frac{6EI_y}{L^2} & 0 \\ & & \frac{12EI_z}{L^3} & 0 & -\frac{6EI_z}{L^2} & 0 & 0 \\ & & & \frac{GI_t}{L}+\left(\frac{12EI_w}{L^3}+\frac{1}{5}\frac{GI_t}{L}\right) & 0 & 0 & -\left(\frac{6EI_w}{L^2}+\frac{3}{30}GI_t\right) \\ & & Symmetric & & \frac{4EI_z}{L} & 0 & 0 \\ & & & & & \frac{4EI_y}{L} & 0 \\ \hline & & & & & & \left(\frac{4EI_w}{L}+\frac{4}{30}GI_tL\right) \end{array}\right] \quad (4a)$$

$$[K]_{j\bar{k}}^{E}=\left[\begin{array}{cccccc|c} -\frac{EA}{L} & 0 & 0 & 0 & 0 & 0 & 0 \\ 0 & -\frac{12EI_y}{L^3} & 0 & 0 & 0 & \frac{6EI_y}{L^2} & 0 \\ 0 & 0 & -\frac{12EI_z}{L^3} & 0 & -\frac{6EI_z}{L^2} & 0 & 0 \\ 0 & 0 & 0 & -\frac{GI_t}{L}-\left(\frac{12EI_w}{L^3}+\frac{1}{5}\frac{GI_t}{L}\right) & 0 & 0 & -\left(\frac{6EI_w}{L^2}+\frac{3}{30}GI_tL\right) \\ 0 & 0 & \frac{6EI_z}{L^2} & 0 & \frac{2EI_z}{L_b} & 0 & 0 \\ 0 & -\frac{6EI_y}{L^2} & 0 & 0 & 0 & \frac{2EI_y}{L_b} & 0 \\ \hline 0 & 0 & 0 & \left(\frac{6EI_w}{L^2}+\frac{3}{30}GI_t\right) & 0 & 0 & \left(\frac{2EI_w}{L}-\frac{1}{30}GI_tL\right) \end{array}\right] \quad (4b)$$

Terms between brackets, related with the formulations including the 7th DOF, also influence the term associated with uniform torsion, located in the position (4,4), being present . With reference to the geometric stiffness matrix, the traditional 6DOFs beam formulations implemented in several commercial FEAPs require the definition of the sole value of the internal axial load. Otherwise, in case of beam formulations including warping, bending moments and bimoment and shear actions significantly contribute to geometric stiffness. Furthermore, these terms strictly depend also on the distance between the load application point and shear center: nil, in case of bi-symmetric cross-section members. Worth noting, whenever structural systems have mono-symmetric cross-section profiles, the definition of all Wagner constants in the geometric stiffness matrix [8] is required for buckling load estimation and set up of an accurate second order analysis.

A few FEAPs offering the 7DOFs beam formulation are available: nevertheless, Authors decided to use ConSteel software as it positively passed several benchmark tests on simulation of the behaviour of non bi-symmetric members in compression or in bending. Moreover, Authors chose ConSteel software because of their expertise in using it.

The warping constant Iw is a variable not included among the input data required to define the 6DOFs FE beam form. It is defined from the theory of sectorial area:

$$I_w=\int \omega^2 dA \quad (5)$$

where is the sectorial area evaluated with respect to the shear center.

In angles, such as in other profiles with plates whose mid-line converges at the same point (e.g. also *T* and *X* profiles), the location of the shear center is at the intersection of the center lines of the legs. Consequently,

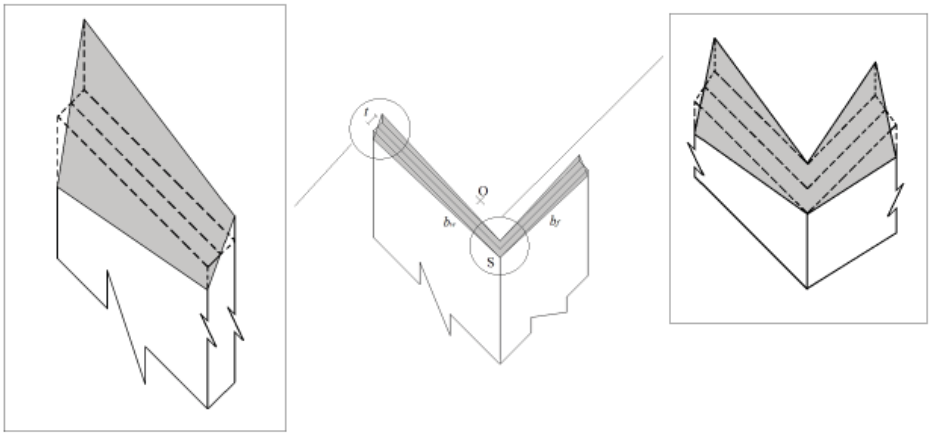

Figure 7: Warping deformation of an angle

there is no warping along the mid-line and the associated sectorial area is nil. For this reason, in routine design engineers assume $I_w = 0$. In a more refined approach, by considering the variability of the warping (and, as a consequence, of the sectorial area) along the thickness of the cross section [12], it is possible to account for the effective distribution of the sectorial area. Effective distribution is linear along the thickness with a zero value in correspondence of the mid-line (figure 7).

Let's consider and an angle having the length of the legs equal to bf and bw (with $b_f < b_w$) and thickness *t*. Than, the maximum sectorial area is equal to:

$$\omega_{max} = b_w \frac{t}{2} \tag{6}$$

By applying eq. 5) to the distribution of the sectorial area showed in figure 6, the warping constant can be defined as:

$$I_w = \frac{t^3}{36}\left(b_f^3 + b_w^3\right) \tag{7a}$$

With the assumption of equal legs, i.e. $b = bw = bf$, the eq. 7a) becomes:

$$I_w = \frac{2b^3 t^3}{36} = \frac{A^3}{144} \tag{7b}$$

where A is the cross-section area.

Once assessed the generalized internal forces for each element, the normal stresses distribution are influenced by axial force, bending moments and bimoment, whose contribution, σ_B, can be appraised by means of the equation:

$$\sigma_B = \frac{B}{I_w}\omega_{max} \tag{8}$$

BUCKLING OF ANGLES

Standard provisions currently adopted for routine steel structures design are based on the concept of the equivalent slenderness [13]. As well-known, it is assumed that, if two structural systems have the same elastic buckling load (i.e., the same slenderness), they also have the same effective load carrying capacity accounting for interaction between instability and plasticity. From a practical point of view, it appears hence of paramount importance to capture, with a more satisfactory degree of accuracy, the elastic buckling load or, equivalently, the buckling load multiplier with respect to the design load condition of interest. This can generally be appraised only by using 7DOFs beam formulation: 6DOFs beam formulations are able to allow for the evaluation of the sole flexural buckling loads of compressed elements, i.e. can be efficiently used to analyse simple frames made by bi-symmetric cross-section members. Consequently, the torsional and flexural-torsional buckling modes cannot be captured, as well as the buckling interaction between axial forces and bending moments: from built-up members to moment-resisting frames, this is of interest for routine design of steel structures. In case of isolated mono-symmetric cross-section members, as alternative to a 7DOFs FE analysis, also worth noting the critical buckling load/multiplier can be appraised by using the expressions proposed in literature [15] and herein proposed, for the sake of simplicity, in Appendix A.

Angles in compression

Let's consider figure 8. For elements under pure compression, stability elastic curves are proposed for 150x15mm equal leg angle, by varying its effective length (Leff) from 400 mm to 2400 mm. Warping displacements and torsional rotation have been considered completely free at both ends. The critical flexural buckling along the principal axes $N_{cr,z}$ and $N_{cr,y}$, the torsional buckling $N_{cr,T}$ and the flexural-torsional one $N_{cr,FT}$, have been appraised by assuming *Iw* equal to *0*, leading hence to a constant $N_{cr,T}$ value independent on the angle length. The flexural-torsional load is the minimum in the initial effective length range (400-1400mm) and then the flexural one, along the weak axis, became the one governing buckling resistance. By using 7DOFs FEAP [6], buckling curve obtained by software is directly associated with the minimum buckling load for each different length. In the same figure, obtained results are presented: they differ less than 1% from those deriving from the set of equations reported in Appendix A.

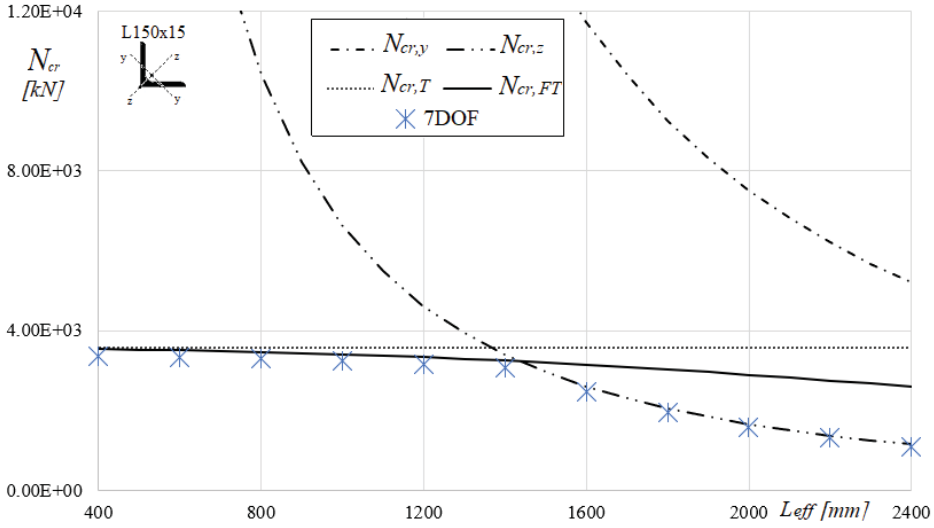

Figure 8: Global elastic stability curve of an agle under pure compression (I_w=0)

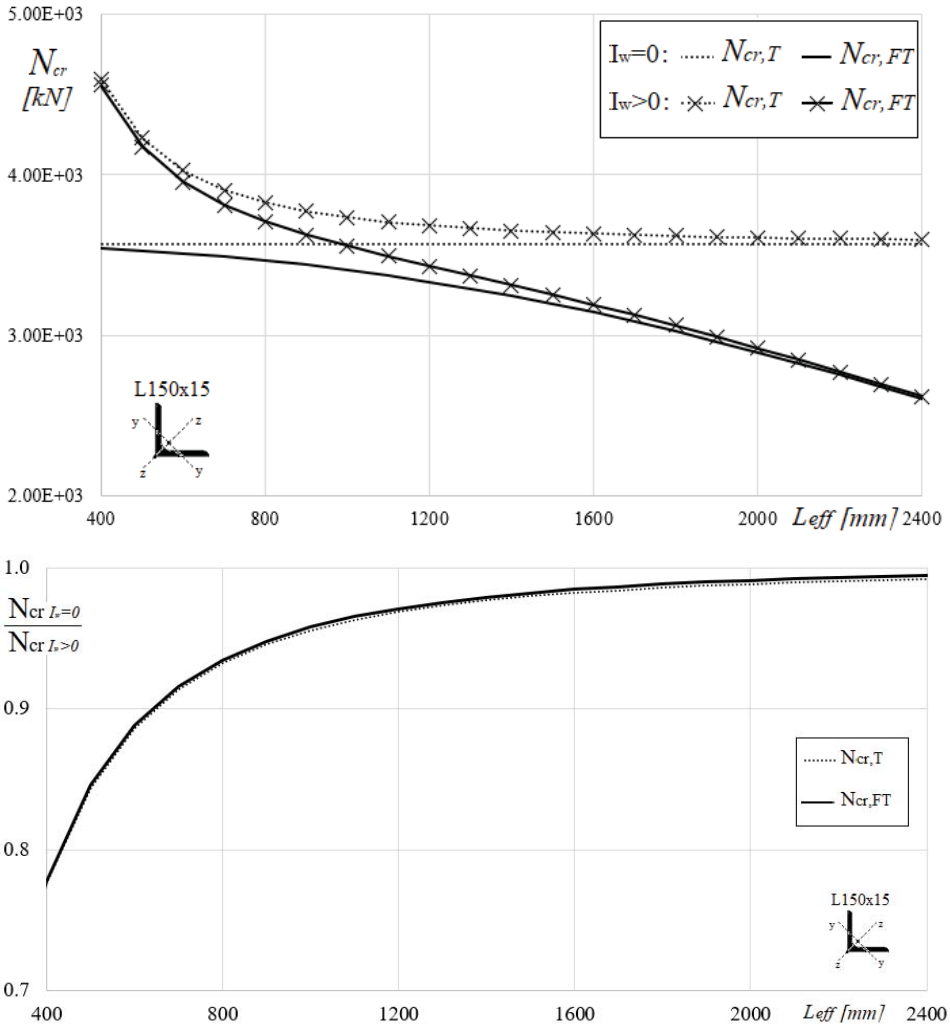

Figure 9: Influence of the warping constant on the torsional and flexural-torsional axial buckling load

The assumption of *Iw=0* leads to underestimate both $N_{cr,T}$ and $N_{cr,FT}$. In Figure 9 the torsional and flexural-torsional buckling curves are plotted, also considering the effective I_w value (dashed lines), i.e. the one obtained via eq. 7). The influence of Iw can be directly appraised in the *b*) part of the same figure, where the buckling load evaluated by assuming $\boldsymbol{I_w=0}$ over the one associated with the effective value ($I_w>0$) nil is plotted versus the effective length. It can be noted that the influence of I_w on $N_{cr,T}$ and $N_{cr,FT}$ is the same and the two curves are practically coincident. Furthermore, differences are non-negligible (up to 70%) only in the initial part of the curve. From ef-

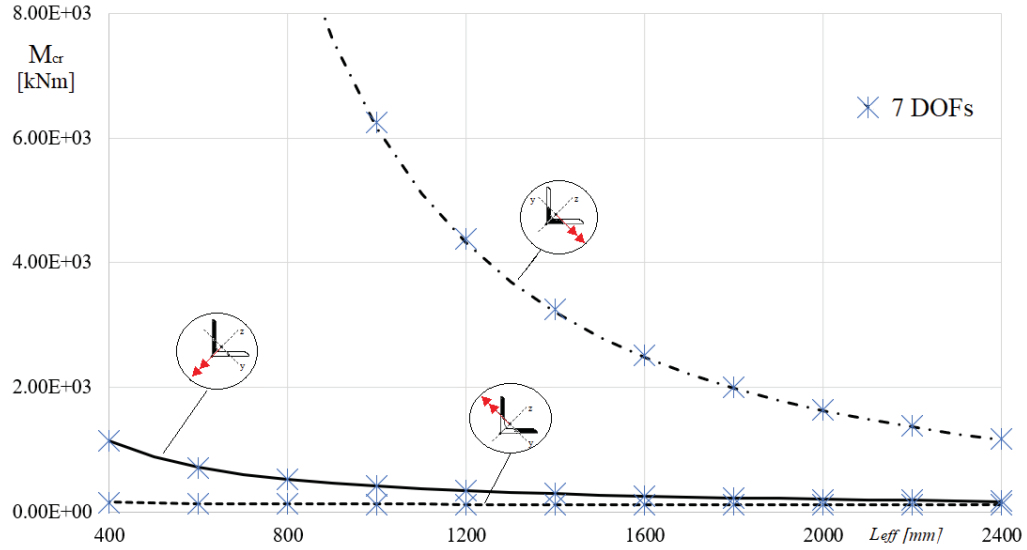

Figure 10: Buckling curve for angle in pure bending (black zones are in compression)

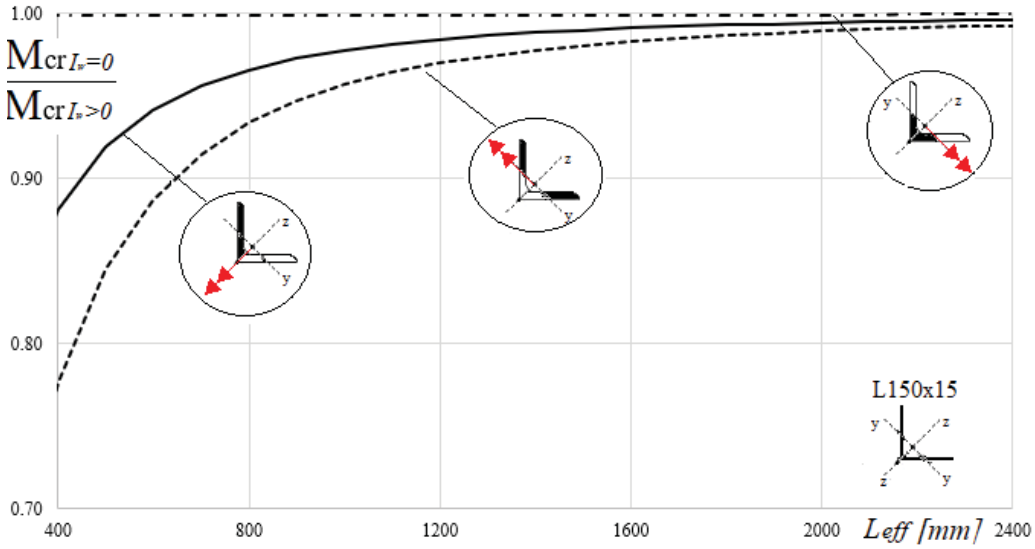

Figure 11: Influence of the warping constant on the bending buckling load

fective length 900 mm and above the become negligible (never greater than 5%), but these cases are, in general, out of interest for practical design purposes, owing to the degree of continuity provided by welded connections. Due to the direct dependence of I_w from the thickness, the smaller the thickness, the lower the importance of considering this value.

Angles in bending

About the buckling response of angles in pure bending (for bending along the y axis), owing to the presence of a single axis of symmetry, the leg ends in tension or compression lead to two different stability curves, as shown in figure 10. The response for bending along the z axis related to the L150x15 mm angle is also plotted presenting the 7DOFs FE results, that, for these cases also , are more than accurate (errors lower than 1%).

The constant warping influence in the critical buckling load for elements in bending can be appraised in figure 11. Unlike for bending along the symmetry axis, in case of bending along the y axis, the influence of Iw cannot be neglected for practical design purposes, especially in cases of short lengths. This influence in more evident in case of leg ends under tension. These curves can be obtained by using the equations proposed in literature [14] and reported in the Appendix A.

Angles under bending and compression

Axial force and bending moment interactions have to be suitably accounted for also in critical elastic conditions, as already discussed in [15], especially in built-up steel components like the one forming derricks, owing to the presence of welded diagonals. The critical axial force-bending moment domains for a double supported L150x15mm angle, having 1250mm of length, subjected to bending moments along *y* or *z* axis, are shown in figures 12 and 13, respectively. In order to provide results of general validity, different linear bending moment

distributions have been considered, i.e. $\Psi=0.5$, $\Psi=0$ and $\Psi=-0.5$, being the ones of interest with respect to the applicative part described in the following. Closed expressions used to obtain these domains are available directly from the literature and proposed in Appendix A. Also, the influence of term I_w is highlighted by using a different line format (dashed line $I_w = 0$ and solid line $I_w > 0$). It can be noted that, with the exception of the zone with lowest values of M_{cr} these relationships are practically linear independently of the bending moment distribution. Furthermore, as expected from the cases previously discussed, I_w influence is really limited, being quite high the effective angle length that has been considered for these domains.

In the y direction, the domain depends on the sign of the bending moment, while in the other bending direction it is the same for positive or negative bending moment distribution. Focusing attention on the case of angle with the leg in compression at the free end (Figure 13), it can be noted that I_w influence is limited and the concavity of the N_{cr}-M_{cr} domain should hamper the use of a linear interpolation because slightly unsafe.

OVERALL DERRICK BUCKLING

As required by EC3 [4], as well as by other provisions dealing with structural steel design, overall buckling analyses have to be at first performed on the structure of interest to appraise the lower buckling load multiplier (α_{cr}). As to the set of considered cases, the values of the buckling load multiplier associated with the 6 and 7DOFs considered FE beam formulation, $\alpha_{cr,6}$ and $\alpha_{cr,7}$ respectively, are reported in table 1 together with the description of the associated buckling modes. With the exception of the four cases characterized by boom inclination at 15°, the α_{cr} differences in terms of critical load multipliers are non-negligible. As expected, $\alpha_{cr,7}$ is significantly lower than $\alpha_{cr,6}$ confirming the importance for angles of the flexural-torsional buckling. The $\alpha_{cr,6}/\alpha_{cr,7}$ ratio ranges, in fact, from 1.3 (B_NS80) to 2.17 (B_NS65).

Furthermore, with the exceptions of A_SB65 and A_SB80, generally the overall buckling modes, that are basically of the three types depicted in figure 14, are independent on the adopted beam formulation. The elastic buckling modes of the built-up component mentioned in

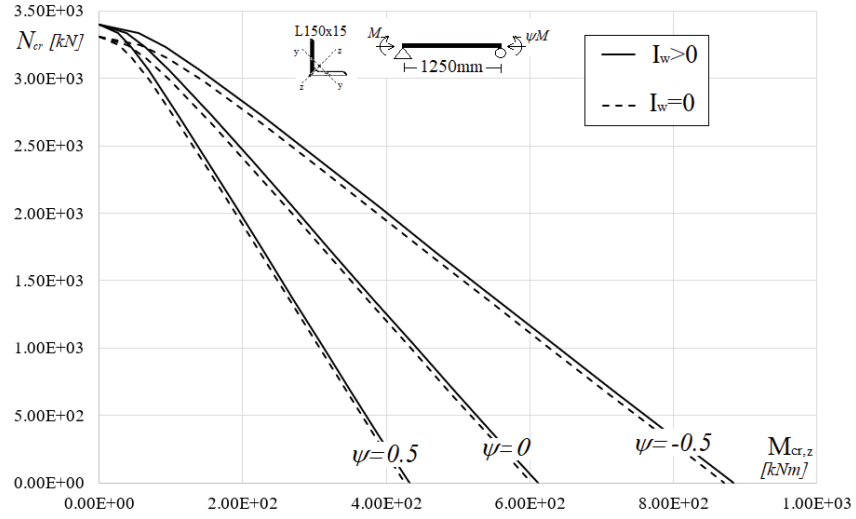

Figure 12: Critical domain for bending moment around z axis, with different linear moment distributions

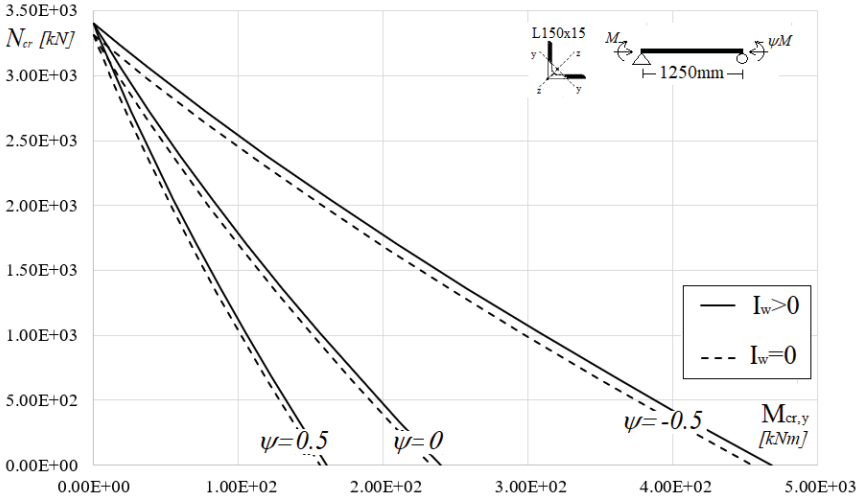

Figure 13: Critical domain for bending moment around y axis, with different linear moment distributions

table 1 correspond to the overall derrick buckling, which are always due to the buckling of diagonal members. As mentrioned, in case of 6DOFs beam formulation only the flexural one is estimated, neglecting bending moment-axial force interactions: this reflects in a high level of overestimation of α_{cr}.

DESIGN ANALYSIS RESULTS

Non-linear analyses by considering only geometrical effects have been performed, also when not required by the EC3 criterion (i.e. for A_SB80 and B_NS65). Moreover, the αcr values (Table 1) indicated that the considered derricks are classified as slender structures with limited influence of second order effects. Key features of the output analysis results are herein shortly discussed.

At first, attention has been paid to the deformability: table 2 presents the ratio between the 7 and 6DOFs displacements along the principal directions (*x, y, z* in figure 4) at the top of the boom and of the tower. In the y-direction, differences at the top of the tower are in general more limited than the ones at the boom top. In case of inclinations at 15°, 6DOFs displacements are always slightly greater than the 7DOFs ones. In the other cases, 7DOFs displacements are in general greater than the 6DOFs ones, up to 18% and 12% for the top of the boom and of the tower, respectively.

For what concerns the influence of the 7th DOF on the axial force distribution along the elements, the output of all FE beams was considered and the differences between

Table 1: Results from global buckling analysis

		$\alpha_{cr,6}$	$\alpha_{cr,7}$	$\alpha_{cr,6}/\alpha_{cr,7}$
A	SB15	6.48 (boom translation)	6.19 (boom translation)	1.05
	SB65	8.19 (boom translation)	5.08 (tower torsion)	1.62
	SB80	10.91 (boom translation)	5.09 (tower torsion)	2.14
	NS15	6.05 (boom translation)	6.05 (boom translation)	1.00
	NS65	6.05 (rod2 torsion)	3.45 (rod2 torsion)	1.75
	NS80	6.58 (rod2 torsion)	3.87 (rod2 torsion)	1.70
B	SB15	6.22 (boom translation)	6.05 (boom translation)	1.03
	SB65	8.30 (tower torsion)	4.63 (tower torsion)	1.79
	SB80	9.15 (tower torsion)	4.61 (tower torsion)	1.98
	NS15	6.05 (boom translation)	6.04 (boom translation)	1.00
	NS65	12.94 (rod2 torsion)	5.95 (rod2 torsion)	2.17
	NS80	8.48 (rod2 torsion)	6.62 (rod2 torsion)	1.28

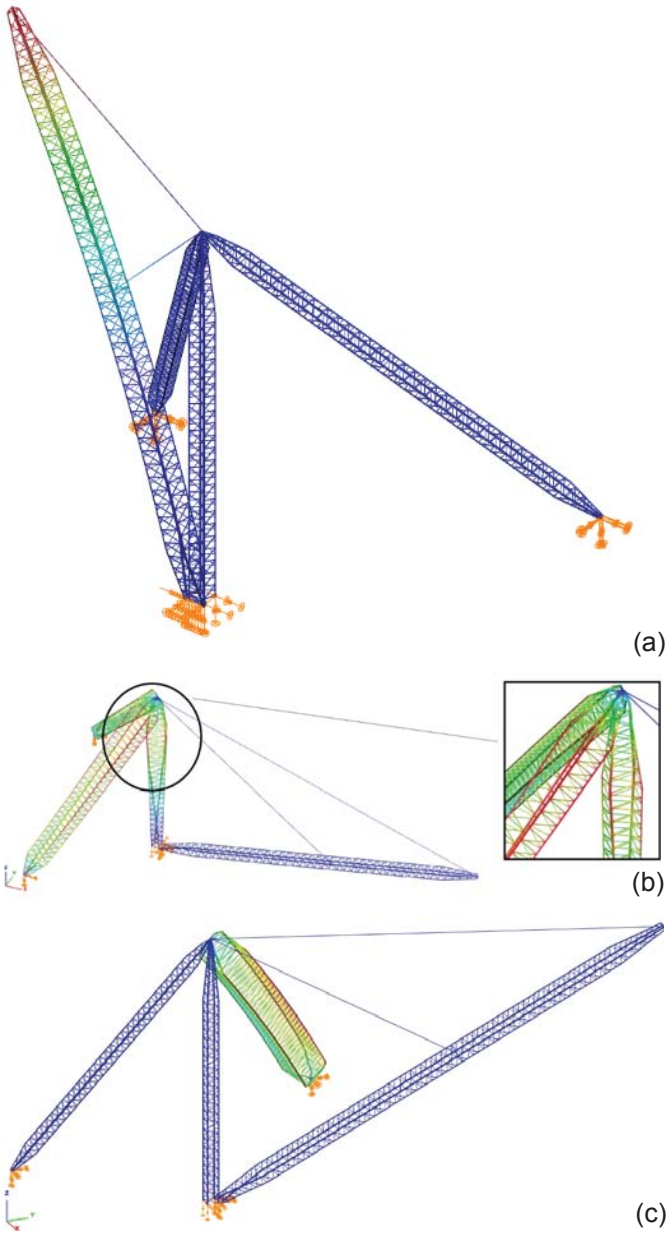

Figure 14: Overall buckling deformed shapes: boom translation (a), tower rotation (b) and rod torsion (c)

N^7_{Ed} and N^6_{Ed} are, in general, quite limited. In table 3 the maximum value of the $\frac{N^7_{Ed}}{N^6_{Ed}}$ ratio, for each component, is reported, grouping together *A* and *B* derrick data. It is worth noting that mean values are close to unity, with the exception of the boom, and the maximum $\frac{N^7_{Ed}}{N^6_{Ed}}$ ratio does not exceed 10% in the rods, 6% in the tower, 9% in the cable and 12% in the boom.

As to the influence of the 7th DOF on the bending moment values, reference has been made for each element, subjected to a linear moment distribution, to the equivalent

Table 2: Comparison in term of displacements

		Top of the Boom			Top of the Tower		
		$\frac{d_x^7}{d_x^6}$	$\frac{d_y^7}{d_y^6}$	$\frac{d_z^7}{d_z^6}$	$\frac{d_x^7}{d_x^6}$	$\frac{d_y^7}{d_y^6}$	$\frac{d_z^7}{d_z^6}$
A	SB15	0.96	0.95	0.91	1.00	0.98	1.00
	SB65	1.05	1.11	1.05	1.06	1.03	1.04
	SB80	1.05	1.14	1.06	1.04	1.04	1.05
	NS15	0.97	1.18	1.06	0.99	0.98	1.00
	NS65	0.97	1.16	0.90	1.06	0.98	1.04
	NS80	0.96	0.96	0.94	1.02	1.02	1.02
B	SB15	0.98	1.00	0.95	1.00	1.00	1.00
	SB65	1.01	1.00	0.98	1.00	0.99	1.01
	SB80	1.02	1.10	1.05	1.02	1.02	1.05
	NS15	0.99	1.12	1.05	1.00	1.10	1.03
	NS65	0.99	1.15	1.04	1.02	1.05	1.03
	NS80	0.95	1.14	1.03	1.00	1.08	1.04

Table 3: Comparison in term of maximum internal axial force $\frac{N_{Ed}^7}{N_{Ed}^6}$

$\frac{N_{Ed}^7}{N_{Ed}^6}$	tower	boom	Tie_ rod1	Tie_ rod2	Cable
SB15 (A+B)	0.96	0.95	0.93	0.94	0.94
SB65 (A+B)	1.06	1.08	1.05	1.05	1.05
SB80 (A+B)	1.06	1.11	1.06	1.05	1.05
NS15 (A+B)	0.97	1.12	1.06	0.91	0.91
NS65 (A+B)	0.97	1.10	0.90	0.97	0.97
NS80 (A+B)	0.96	0.96	0.94	0.94	0.94
mean	1.00	1.08	0.99	1.03	1.02

non dimensional bending moment $m_{eq,j}$ defined as:

where *j* indicates the principal axis of reference (i.e. *j=y* or *j=z)*, $M_{a,j}$ and $M_{b,j}$ are the end moments (with $M_{a,j}>M_{b,j}$) and $M_{pl,j}$ is the plastic bending resistance of the angle.

$$m_{eq,j} = (0.6\ M_{a,j} + 0.4\ M_{b,j})/M_{pl,j} \quad (9)$$

It is worth noting that $m_{eq,j}$ also directly allows for an appraisal of the effect of the moment on the angle resistance.

Key results are depicted in figure *15:* $m^7_{Bq,j}$ and $m^6_{Bq,j}$ points are plotted for boom (a), tower (b) and tie-rods (c). Data are distinguished considering the three different boom inclinations; if the representative point has the abscissa greater than the ordinate, so the use of 6DOFs formulation is unsafe, otherwise the bending resistance contribution is over-estimated. In the same figure, the bisector (solid) line, corresponding to a zero difference between the two compared formulations and dashed lines, corresponding to differences of ±30% and ±70%, are also plotted. As a general remark, a non-negligible percentage of points is characterized by $m^7_{Bq,j}$ greater than $m^6_{Bq,j}$: 61% for boom and towers, approximately, and 46% for tie-rods. In case of z bending moment, the corresponding percentages are 36% (boom), 50% (tower) and 37% (tie-rods). Furthermore, in general the differences between $m^7_{Bq,j}$ and $m^6_{Bq,j}$ are, worth noting, quite limited. Indeed, the base of data is 13330 points (4800 points for the boom, 1450 for the tower and 7570 for the tie-rods) but only few points are far from the origin. By considering a threshold value of 0.1, only 6% and 4% of data exceed this limit for the y and z bending direction, respectively.

An important aspect of the 7DOF analysis is related to the bimoment presence, leading, according with eq. 8), to an additional normal stress (σ_B that, in some cases, results non-negligible if compared with the yielding (f_y) of the material. In table 4, the $\frac{\sigma_B}{f_y}$ ratio is presented in terms of maximum (max) and mean value for each component. It can be noted that, if mean values are considered, the contribution of the bimoment is in general negligible. Otherwise, peak values are limited in the tower, but in the other elements can reach 13% of the yielding: a non-negligible percentage from an engineering point of view.

CONCLUDING REMARKS

The present paper deals with stiffleg derricks with angles, whose design is usually carried out by means of FEAPs offering the traditional 6DOFs beam formulation. Angles, such as channels and cross-section elements with a sole symmetry axis, require for the structural analysis a more refined 7DOFs beam formulation, able to account for the the effects associated with warping torsion, as well as for the coupling between axial force and bending moments.

Buckling of angles is often governed by the flexural-torsional mode that, if neglected, can lead to a non-negligible overestimation of the critical loads. Furthermore, the common assumption of warping constant nil ($I_w = 0$) leads to moderately underestimate the criticalbuckling loads associated with the torsional and flexural-torsional instability. This assumption also gives an excessive approximation regarding the resistance and stability checks, since the non-negligible contribution of the bimoment is neglected in routine design.

Two derricks, have been considered and, despite two different panel configurations, common outcomes can be proposed. As to the overall buckling, due to the impossibility of the FEAPs to capture buckling modes associated

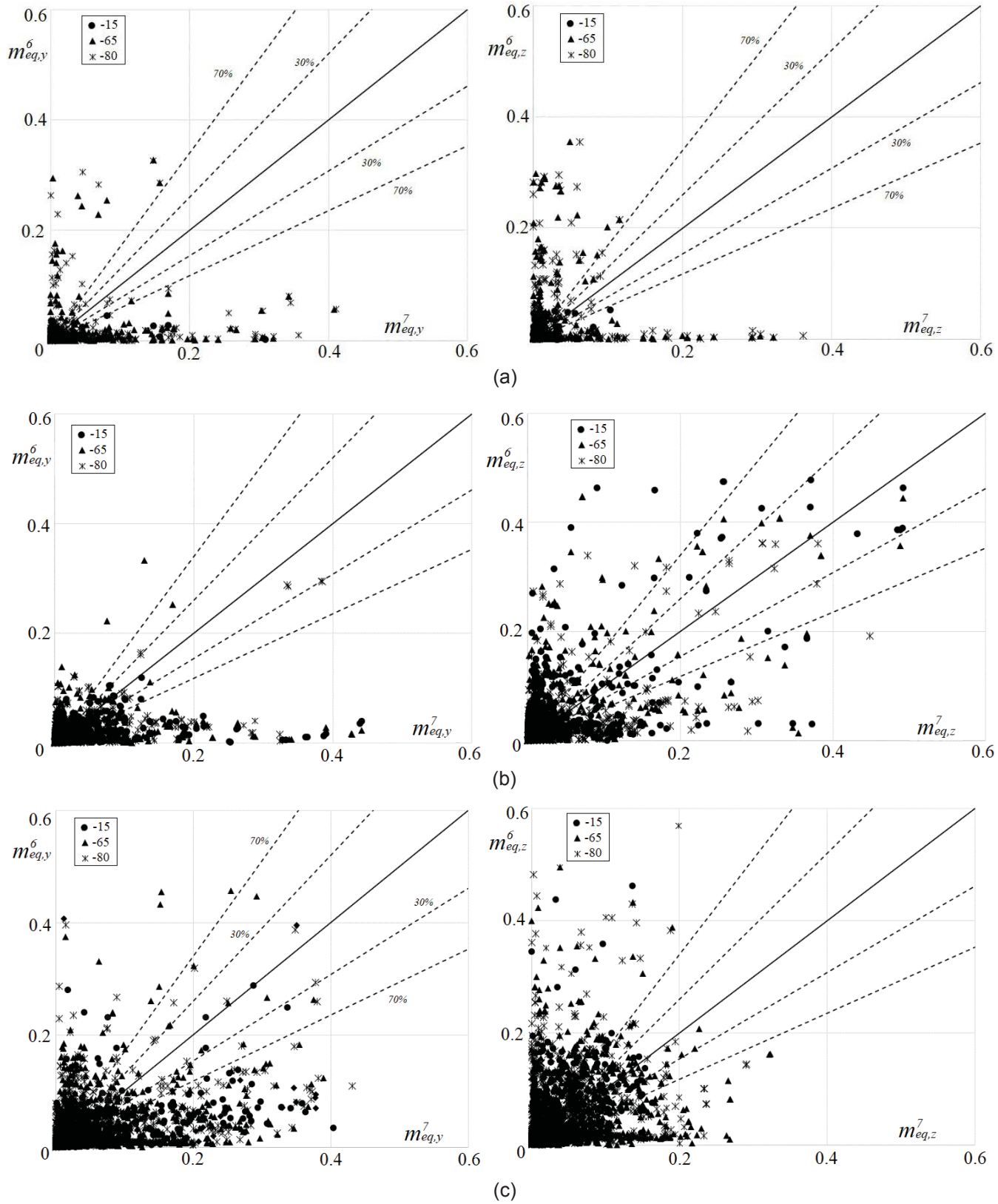

Figure 15: Non dimensional bending moment 6 vs 7DOFs for: a) boom, b) tower and c) tie-rods

with torsional and flexural-torsional instability of the single angle, load multiplier can be overestimated up to two times, as demonstrated with reference to the considered derricks. Moreover, the differences between the equivalent bending moment observed from the 6 and 7DOFs results confirm the need of using the more refined FE beam formulation. 7 DOFs formulation is also essential to capture the bimoment, that in few cases cannot be neglected for a safe design.

Table 4: Influence of bimoment

	$\frac{\sigma_B}{f_y}$[%]		tower	boom	Tie rod1	Tie rod2
A	SB15	max	2.1	13.2	7.0	7.7
		mean	0.1	1.0	0.6	0.7
	SB65	max	0.7	14.5	14.6	13.2
		mean	0.7	1.4	1.2	1.1
	SB80	max	1.2	15.2	13.2	13.8
		mean	0.4	1.5	1.2	1.1
	NS15	max	2.8	13.2	7.0	7.7
		mean	0.1	1.1	0.6	0.7
	NS65	max	4.9	15.1	13.9	13.9
		mean	0.1	1.5	1.2	1.1
	NS80	max	6.3	15.7	13.2	12.5
		mean	0.1	1.4	1.1	1.0
B	SB15	max	1.5	14.5	6.5	7.8
		mean	0.1	1.2	1.1	1.2
	SB65	max	1.0	13.5	13.5	13.5
		mean	0.5	1.4	1.5	1.2
	SB80	max	0.9	14.6	14.0	13.3
		mean	0.5	1.3	1.1	1.3
	NS15	max	2.1	15.2	6.5	7.5
		mean	0.1	1.1	0.8	1.5
	NS65	max	3.5	13.4	13.5	13.1
		mean	0.2	1.3	0.9	1.3
	NS80	max	3.3	13.5	14.5	14.5
		mean	0.1	1.3	0.7	1.1

Finally, it can be concluded that it would be desirable that standard codes dealing with the design of structures having mono-symmetric cross-section members should be improved by specifying the minimum requirement of the FEAPs as well as by including the bimoment contribution in the verification checks.

REFERENCES

1. L. K. Shapiro, J. P. Shapiro, “Cranes and derricks”. McGraw-Hill Education, 4th edition, 2010. ISBN: 9780071625579 007162557
2. UCIMU, “Guide to application of the Machinery Directive 2006/42/EC”. Edizioni TNE, 2nd edition, 2017.
3. L. Solazzi, N. Zrnic “Design of a high capacity derrick crane considering the effects induced by load application and release”, Journal of Applied Engineering Science 15(1), 409, 15-24, 2017. doi: 10.5937/jaes15-11930.
4. EN1993-1-1, Eurocodice 3 “Design of steel structures – Part 1-1: General rules and rules for builsings”, CEN 2015.
5. Sap2000 v.19, FE software, https://www.csiamerica.com/, accessed 2019.
6. ConSteel v. 13, FE software, http://www.consteel-software.com/en, accessed 2019.
7. K. Bathe, E.L. Wilson “Numerical Methods in Finite element analysis” Prentice-Hall, 1976. doi: 10.1002/nme.1620110913.
8. W. F. Chen, T. Atsuta, “Theory of beam-columns: Vol. 2 Space Behaviour and Design”. McGraw Hill, New York, 1977.
9. V. Z. Vlasov, “Thin-walled elastic beams”. Published for The National Science Foundation, Washington D.C., by the Israel Program for Scientific Translations, Jerusalem, 1961.
10. C. Bernuzzi, A. Gobetti, G. Gabbianelli, M. Simoncelli, “Warping influence on the resistance of uprights in steel storage racks”. Journal of constructional steel research, 101, pp. 224-241, 2014. doi: 10.1016/j.jcsr.2014.05.014.
11. C. Bernuzzi, N. Draskovic, M. Simoncelli, “European and United States approaches for steel storage pallet rack design. Part 2: Practical applications”, Thin-walled structures, 97, pp. 321-341, 2015. doi: 10.1016/j.tws.2015.08.011.
12. F. Bleich, “Buckling strength of metal structures”. Engineering societies monograph, McGraw Hill, New York, 1952. ISBN 10: 0070058903.
13. G. Ballio, F.M. Mazzolani, “Theory and design of steel structures”, Chapman and Hall, London, 1983. ISBN: 0412236605.
14. F. Mohri, N. Damil, M. Potier-Ferry, “Buckling and lateral buckling interaction in thin-walled beam-column mono-symmetric cross section”. Applied Mathematical Modelling, 37 (5), pp. 3526-3540, 2013. doi: 10.10316/j.apm.2012.07.053.
15. C. Bernuzzi, B. Cordova “Structural steel design to Eurocode 3 and AISC specifications” Wiley Blackwell, United Kingdom, 2016. ISBN 10: 1118631285
16. C. Bernuzzi, M. Simoncelli, “EU and US approaches for steel storage pallet racks with mono-symmetric cross-section uprights”, Thin-walled structures, 113, pp. 181-204, 1April 2017. doi: 10.1016/j.tws.2017.01.014.

APPENDIX A: EXPRESSIONS AND DEFINITION OF THE M_{cr} - N_{cr} DOMAINS

The elastic critical buckling load for an angle under compression is the minimum between:

Flexural buckling. The cross-section in the deformed shape move into one of its principal directions (*y* and *z*, in the paper) and the critical load $N_{cr,F}$ is defined as:

where *E* is the Young’s modulus, I_y and I_y are the second moment of area along the principal directions and L_y and

L_z are the associated effective buckling lengths.

$$N_{cr,F}=min\left\{N_{cr,y}=\frac{\pi^2 E I_y}{L_y^2};N_{cr,z}=\frac{\pi^2 E I_z}{L_z^2}\right\} \quad \text{(A1)}$$

Torsional buckling. The cross-section rotates around its shear center differing from the centroid in angles. The critical load $N_{cr,T}$ is defined as:

where:

where G is the shear modulus, I_t is the Sant venant constant, I_w is the warping constant, i_y are i_z are the sectional

$$N_{cr,T}=\frac{1}{i_0^2}\left[G I_t+\frac{\pi^2 E I_w}{L_T^2}\right] \quad \text{(A2a)}$$

radii, L_T is the torsional buckling length, z_s is the shear

$$i_0^2=i_y^2+i_z^2+z_s^2 \quad \text{(A2b)}$$

center distance from the centroid of the cross-section.

Flexural-torsional buckling. Is a combination of the previous dedormed shapes. The cross section rotates around its shear centre and move along the simmetry axis. For angles with z as the symmetry axis, the critical load $N_{cr,FT}$ is defined as:

where:

The elastic critical moment for an element under pure bending (M_{cr}), referred to a simply supported angle, can

$$N_{cr,FT}=\frac{N_{cr,z}}{2\beta}\left[1+\frac{N_{cr,T}}{N_{cr,z}}-\sqrt{\left(1-\frac{N_{cr,T}}{N_{cr,z}}\right)^2+4(1-\beta)\frac{N_{cr,T}}{N_{cr,z}}}\right] \quad \text{(A3a)}$$

be derived from equation:

$$\beta=1-\left(\frac{z_s}{i_0}\right)^2 \quad \text{(A3b)}$$

- L lenght of the beam between two support;
- E, G Young and shear moduli;
- C_1, C_2, C_3 coefficients to consider the actual distribution of the bending moment along the element.
- z_g distance between the point of applied load and the shear centre of the profile;
- k_z,k_w boundary condition related to the lateral displacements and warping;
- I_z second moment of area around the axis of buckling;
- I_w warping torsion;
- I_t Sant Venant torsion;
- β_y Wagner terms account for the non-symmetri of the profiles

The equation B1 must be referred cse by case to the bending direction. Considering for example a simply supported angle members (k_z = k_w = *1*) with a constant bending moment distribution along its lenght (C_1 = *1*), it is possible to calculate 3 different critical moment, as showed in table B1: 1 for the flexure around z-z and 2 for the flexure around y axis (Table A1).

In the first case Wagner term is equal to 0 being defined as:

Instead in the second case the sign of the Wagner term changes with the change of the sign of the applied bend-

$$\beta_z=\int y\left(z^2+y^2\right)dA=0 \quad \text{(A5a)}$$

ing moment, being the positive axis oriented to the compressed zone:

Moreover, the elastic critical moment for an element un-

$$\beta_y=\int z\left(z^2+y^2\right)dA\neq 0 \quad \text{(A5b)}$$

der pure bending (M_{cr}) and axial force (N), referred to a simply supported angle, can be derived from equation (A6a).

$$M_{cr}=C_1\frac{\pi^2 E I_z}{(k_z L)^2}\cdot\left\{\sqrt{\left(\frac{k_z}{k_w}\right)^2\frac{I_w}{I_z}+\frac{(k_z L)^2 G I_t}{\pi^2 E I_z}+\left(C_2 z_g+C_3\frac{\beta_y}{2}\right)^2}-\left(C_2 z_g+C_3\frac{\beta_y}{2}\right)\right\} \quad \text{(A4)}$$

$$M_{cr}=C_1\frac{\pi^2 E I_z}{(k_z L)^2}\cdot\left\{\sqrt{\left[\left(\frac{k_z}{k_w}\right)^2\frac{I_w}{I_z}+\frac{(k_z L)^2 G I_t}{\pi^2 E I_z}\right]f_M(N)+\left(C_2 z_g-C_3\frac{\beta_y}{2}\right)^2}-\left(C_2 z_g-C_3\frac{\beta_y}{2}\right)\right\} \quad \text{(A6a)}$$

Table A1: Expression of critical buckling moment for an angle under constant moment

	Critical moment	
bending z buckling y	$M_{cr}=\frac{\pi^2 E I_y}{(L)^2}\cdot\left\{\sqrt{\frac{I_w}{I_y}+\frac{(L)^2 G I_t}{\pi^2 E I_y}}\right\}$	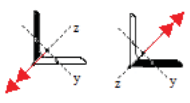 $\beta_z = 0$ $\beta_z = 0$
bending y buckling z	$M_{cr}=\frac{\pi^2 E I_z}{(L)^2}\cdot\left\{\sqrt{\frac{I_w}{I_z}+\frac{(L)^2 G I_t}{\pi^2 E I_z}+\left(C_3\frac{\beta_y}{2}\right)^2}-\left(C_3\frac{\beta_y}{2}\right)\right\}$	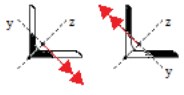 $\beta_y > 0$ $\beta_y < 0$

Where the reduction factor $f_M(N)$ is a function of the acting axial load N and of the critical load for compressed members:

$$f_M(N)=\left(1-\frac{N}{N_{cr,z}}\right)\left(1-\frac{N}{N_{cr,FT}}\right), \quad \text{(A6b)}$$

Where $N_{cr,FT*}$ is equal to:

$$N_{cr,FT*}=\frac{N_{cr,z}}{2\beta}\left[1+\frac{N_{cr,T}}{N_{cr,z}}+\sqrt{\left(1-\frac{N_{cr,T}}{N_{cr,z}}\right)^2+4(1-\beta)\frac{N_{cr,T}}{N_{cr,z}}}\right] \quad \text{(A6c)}$$

The typical N_{cr}-M_{cr} domain represented, like the one in figure 13, can be obtained by a direct procedure which can be summarized in the following steps:

- evaluation of the of N_{cr};
- evaluation of M_{cr};
- define a suitable number of values of the axial force and evaluate the associated critical buckling to make reference to, at least, to the following values: 98%, 95%, 90%, 60%, 40% and 20% of N_{cr}.

This procedure in case of angles leads to three different domains depending on the axial and the versus of bending, according to table A1. The complete element stiffness and geometrical matrixes have been discussed deeply in [10,11].

Paper submitted: 16.12.2019.
Paper accepted: 27.07.2020.